Appl. Phys. A (2017) 123:155
DOI 10.1007/s00339-017-0797-5

Applied Physics A
Materials Science & Processing

Chemical synthesis and characterization of bismuth oxychloride BiOCl nanoparticles

Francisco Miguel Ascencio-Aguirre[1,2] · Lourdes Bazán-Díaz[1,2] · Rubén Mendoza-Cruz[1,2] · Maricela Santana-Vázquez[1,2] · Oscar Ovalle-Encinia[1] · Alfredo Gómez-Rodríguez[2] · Raúl Herrera-Becerra[2]

Received: 4 August 2016 / Accepted: 19 January 2017 / Published online: 10 February 2017

Abstract Bismuth oxychloride (BiOCl) nanoparticles were synthesized using bismuth nitrate pentahydrate ($Bi(NO_3)_3$*$5H_2O$) and tannic acid ($C_{76}H_{52}O_{46}$), the latter playing the role of stabilizing agent in a highly acid environment. For the characterization of the particles several techniques were used. The X-ray diffraction patterns (XRD) confirmed the formation of BiOCl nanocrystals with an average size of 15.33 ± 0.16 nm. Raman spectroscopy showed the characteristic A_{1g} and E_g vibrational normal modes of BiOCl. Through electron microscopy studies (SEM and TEM) the formation of nanosized particles was confirmed. The average particle size measured from TEM images was 22.11 ± 0.29 nm, in good agreement with the one calculated from XRD data. The synthesis method was performed in aqueous solution and it represents an easy and low-cost protocol for the production of BiOCl nanoparticles.

1 Introduction

Bismuth oxychloride (BiOCl) is a useful material with manifold applications such as make-up pigments, pharmaceutical industry, batteries [1, 2], photocatalysis [3], optoelectronic and photovoltaic materials as lighting diodes, lasers, and solar cells, degradation of organic pollutants [4], CO_2 photo reduction [5], etc. This ternary compound in the V–VI–VII families shows p-type indirect gap semiconducting properties [6]. Bismuth oxychloride crystallizes in a tetragonal unit cell with a PbFCl-type structure [7]. The lattice parameters are $a = b = 0.389$ nm and $c = 0.737$ nm, such that Cl^- and $Bi^{3+}O^{2-}$ ions are present in alternate form in the crystalline structure forming two kinds of inverted pyramids, the first with 4 Cl^- ions surrounding the Bi^{+3}, and the other with 4 O^{2-} ions surrounding the Bi^{+3} (Fig. 1c) [8]. This compound has a unique blend of optical, catalytic, and electric properties. Due to its extensive potential applications, it is of importance to be able to obtain BiOCl using novel simple and low-cost methods.

There have been many studies regarding the synthesis of BiOCl where different procedures such as wet chemistry [9, 10], chemical vapor deposition (MOCVD) [11], combustion method [12], sol–gel template [13] under hydrothermal condition [14], synthesis in the presence of PVP [15], simple hydrolysis method [16], one-step alcohol-heating method [17], ball-milling [18], solvothermal method [19, 20], etc. were used. In a similar vein diverse morphologies have been reported for the synthesized particles such as nanoflakes [21], nanosheets [22], microspheres [23], microflowers [24], nanoplates [25], nanodisks [26] etc. All these methods use, in some way or another, thermal treatments at temperatures higher than 60 °C in order to reach the final stage of the particles. The aim of this work is to present a synthesis method for BiOCl nanoparticles that is simple, economic, and free from thermal treatments.

2 Experimental procedure

The BiOCl nanoparticles were synthesized through a preparation method previously reported by our group [27]. For

✉ Francisco Miguel Ascencio-Aguirre
fascencio@fisica.unam.mx

[1] Posgrado en Ciencia e Ingeniería de Materiales, UNAM, Circuito de la Investigación Científica, Ciudad Universitaria, C.P. 04510 México, Mexico

[2] Departamento de Materia Condensada/Instituto de Física UNAM, Circuito de la Investigación Científica, Ciudad Universitaria, C.P. 04510 México, Mexico

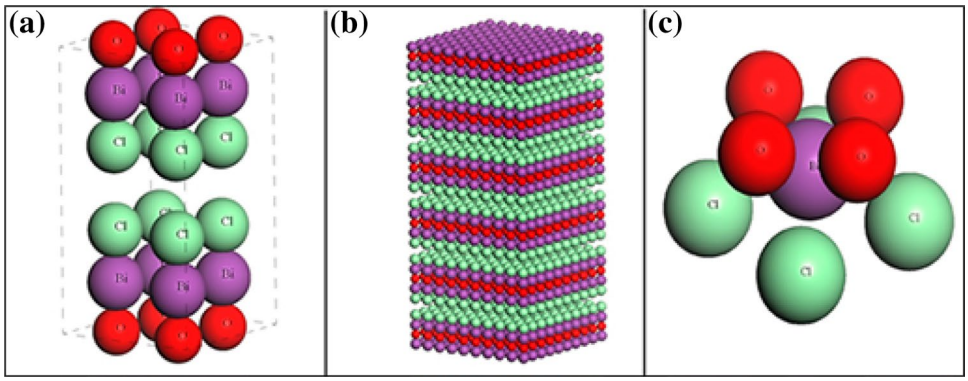

Fig. 1 Atomic models of the BiOCl structure: **a** BiOCl tetragonal unit cell. **b** 5×5×5 supercell in which the alternated layers of Bi, O, and Cl are easily distinguished. **c** Inverted pyramids in the BiOCl

the present report, we implemented an additional protocol consisting in a lyophilization process of the final solution [28] to get a fine powder for characterization. The lyophilization procedure started with the rapid freezing of the solutions with liquid nitrogen ($T=77$ K), followed by the elimination of the liquid phase under low pressure till solid state (powder) samples were obtained. It has been observed that tannic acid plays a stabilizing role for the production of NPS β-Bi_2O_3, see for instance [29]. In this work we prepared simultaneously two aqueous solutions; the first was tannic acid ($C_{76}H_{52}O_{46}$) (Aldrich >99.999%) in distilled water at 0.45 mM concentration, and in order to obtain a highly acid environment a 0.1 M HCl solution was added till a pH = 2 was obtained. The second solution was bismuth nitrate pentahydrate (Bi $(NO_3)_3$*$5H_2O$) (Aldrich 99.999%) at 3 mM concentration. Immediately afterwards an ultrasonic bath was performed for 5 min to homogenize both solutions. Then, both solutions were mixed (50:50 ml) and the solution was then frozen with liquid nitrogen in order to lyophilize and thus obtain powder samples.

2.1 Characterization

The powder samples were characterized by X-ray diffraction (XRD) with a diffractometer Bruker, D8 Advance with a Cu-Kα (1.54059 Å) radiation source operating at 34 kV and 30 mA being used to identify the crystalline phase. The samples where measured in a 2-theta range of 20°–120° with a step size of 0.02°. The phase was identified using the Joint Committee Powder Diffraction Standards (JCPDS) and Crystalline structure was refined with the Rietveld method using the BGMN program [30] and the graphical interface Profex [31]. Peak profiles were modeled with a Lorentzian function to determine the crystal size anisotropy using the Debye–Scherrer formula [32] and spherical harmonics as base functions to model the reflection width parameters as functions of the Miller indices of the reflection. The Raman spectra were obtained in a Thermo Scientific confocal microscope equipped with Micro-Raman using λ = 532, 633, and 780 nm lasers, where the measurements were carried out in the 3000–50 cm^{-1} range. Scanning electron microscopy (SEM) and energy-dispersive X-ray spectroscopy (EDS) studies were performed in a Hitachi S-5500 microscope operating at 30 kV. Finally, for transmission electron microscopy (TEM) the sample was prepared depositing the powder onto a 300 mesh Cu grid, and the analysis was performed in a JEOL JEM-2010F FasTem microscope operated at 200 kV, with an ultrahigh resolution polepiece, and a spherical aberration coefficient of $C_s = 0.5$ mm.

3 Results and discussion

3.1 XRD

After lyophilizing the solution (sample already in powder form), we study the crystallographic structure of the nanoparticles through XRD characterization. Figure 2 shows the Rietveld refinement plot of BiOCl nanoparticles. From Rietveld refinement we observe unique phase of BiOCl with 100 wt%. The XRD where identified and modeled with tetragonal BiOCl (JCPDS: 96-901-1783) described by the space group P4/nmm (129). The average crystal size was 15.33 ± 0.16 nm. The cell parameters were calculated and the resulting lattice parameters were $a = 3.8861 \pm 0.0021$ and $c = 7.3782 \pm 0.0042$ in Å units, according to the space group, oxygen atom positions are fixed in unit cell, while bismuth and chlorine atoms have variable z coordinates. Atomic position refined as a fraction of the lattice parameters were $Bi_z = 0.1725 \pm 0.0003$ and $Cl_z = 0.657 \pm 0.0017$. Finally the residues were as follows: $R_{wp} = 6.61\%$, $R_{exp} = 5.60\%$, and $R_{wp}/R_{exp} = 1.18$.

3.2 Raman spectroscopy

Raman spectra were measured to obtain information on vibrational normal modes of the samples and to do a more detailed analysis. Three different lasers ($\lambda = 532$, 633, and 780 nm) were used for the characterization. Assuming that

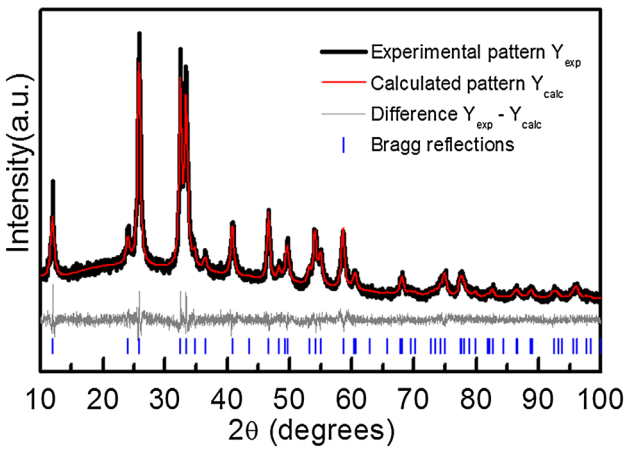

Fig. 2 X-ray diffraction. The *continuous black line* is the experimental data; the *red line* superposed is the calculated pattern. At the *bottom* of the diagram, the difference between the experimental and calculated points is shown (*gray*). Vertical *blue marks* at the *bottom* are displayed corresponding from to the Bragg positions for the BiOCl nanoparticles phase. The background was modeled with a Lagrangian polynomial

our compound has tetragonal symmetry with space group *P4/nmm* and that into each unit cell there are two molecules (Fig. 1a), we see that this compound will display the $\Gamma = 2A_{1g}+2A_{2u}+B_{1g}+3E_g + 2E_u$ vibrational modes of which only two (A_{1g} and B_{1g}) are Raman active. The remaining normal modes of vibration are located in the IR region. In previous studies stretching modes (A_{1g}) have been found which are related to the Bi–Cl bond.

In Fig. 3a the measured spectrum for $\lambda = 532$ nm is presented where a systematic shift towards higher Raman frequencies is observed. The signal corresponding to the A_{1g} vibration (found at 62.7 cm^{-1}) displays a shift of about 4.2 cm^{-1} with respect to the value reported by A. Rulmont [33]. Similarly, the 146.9 cm^{-1} peak, related to the Bi–Cl A_{1g} internal stretching mode, displays a shift of 2.9 cm^{-1} with respect to the one found, and lastly, the 202.8 cm^{-1} peak, corresponding to E_g, shows a 2.3 cm^{-1} with respect to the one reported. These shifts might be related to phononic confinement effects.

When measuring with the $\lambda = 633$ nm laser we observed again that the spectrum peaks show a systematic shift of about 9.2, 9.1, and 12.1 cm^{-1} for the A_{1g} and E_g modes, respectively; such a Raman shift was attributed to the laser power. In addition we show the $\lambda = 780$ nm measured spectrum which significant peak is not observed.

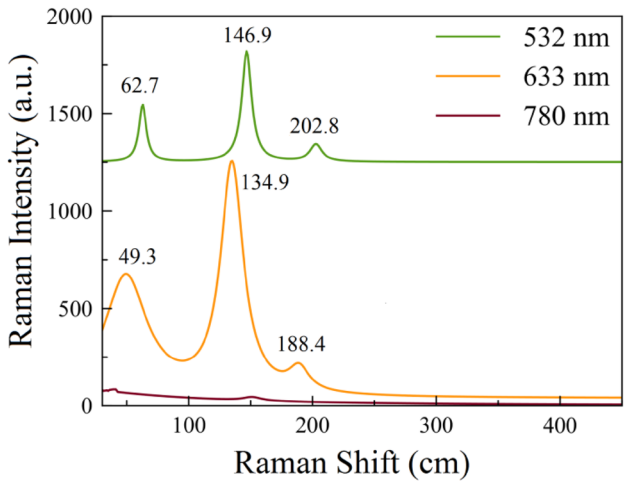

Fig. 3 Raman spectra for three different wavelengths

3.3 Electron microscopy

3.3.1 Scanning electron microscopy (SEM)

SEM images are shown in Fig. 4. We noticed a large number of small individual particles within a matrix which was associated to the precursor's agent. The elemental analysis EDS of these particles confirmed the presence of Bi, Cl, and O (Inset in Fig. 4b). The weight percentage of the elements corresponded to Bi = 53.62%, O = 34.11%, and Cl = 12.27%. The aluminum and copper signals came from the holder and the grid in which the sample was mounted. The high content of oxygen was attributed to a large amount of OH groups present in the tannic acid, which served not only as the stabilizing agent, but as a matrix where nucleation and growth of particles can occur.

3.4 Transmission electron microscopy (TEM)

In Fig. 5 a low magnification TEM image and its corresponding electron diffraction pattern (EDP) are shown. After indexation of the EDP, the BiOCl crystal structure of the samples was confirmed. The (0 0 2), (0 1 1), (0 0 3), (1

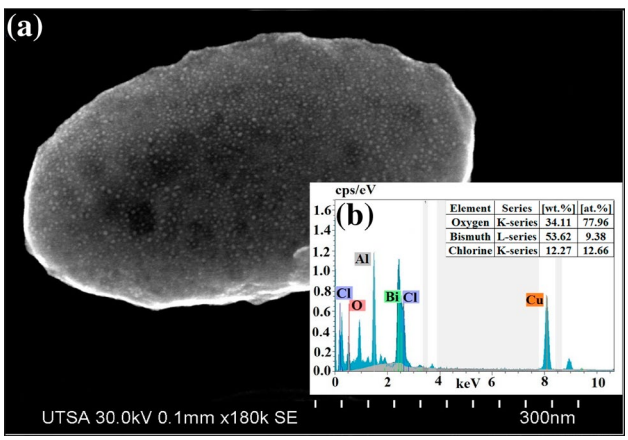

Fig. 4 **a** SEM Images, **b** EDX analysis

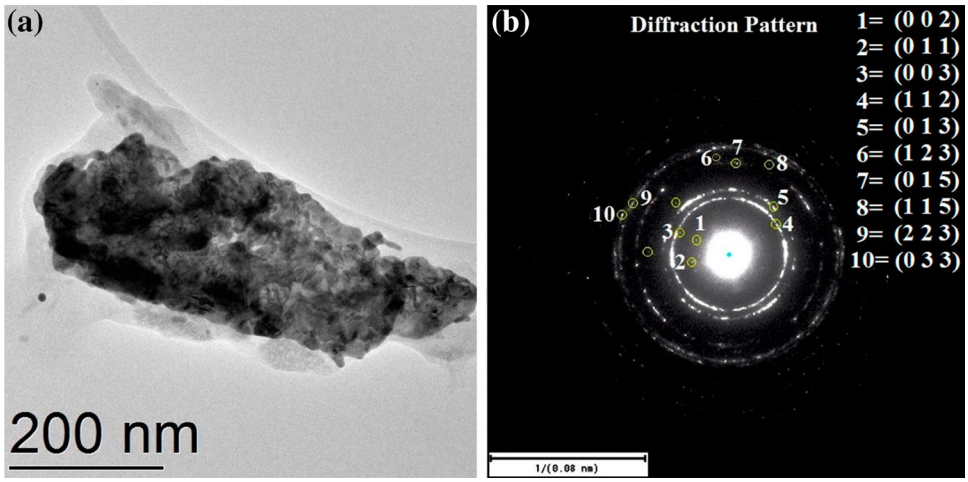

Fig. 5 **a** Low magnification TEM image, **b** diffraction pattern

1 2), (0 1 3), (1 2 3), (0 1 5), (1 1 5), (2 2 3), and (0 3 3) lattice planes are indicated (JCPDS, # 96-901-1783).

Although agglomeration of nanoparticles could be present as it was evident from Fig. 5, dispersed and well-defined particles were found in the sample. Figure 6a–c shows TEM images of roughly spherical particles. However, high magnification images enabled us to observe the faceted nature of these nanoparticles, which are not perfectly spherical (Fig. 6c). A size histogram was done based on 1809 particles and it is presented in Fig. 6d. The mean size was calculated to be 22.11 ± 0.29 nm and a mode of about 8 nm having a good

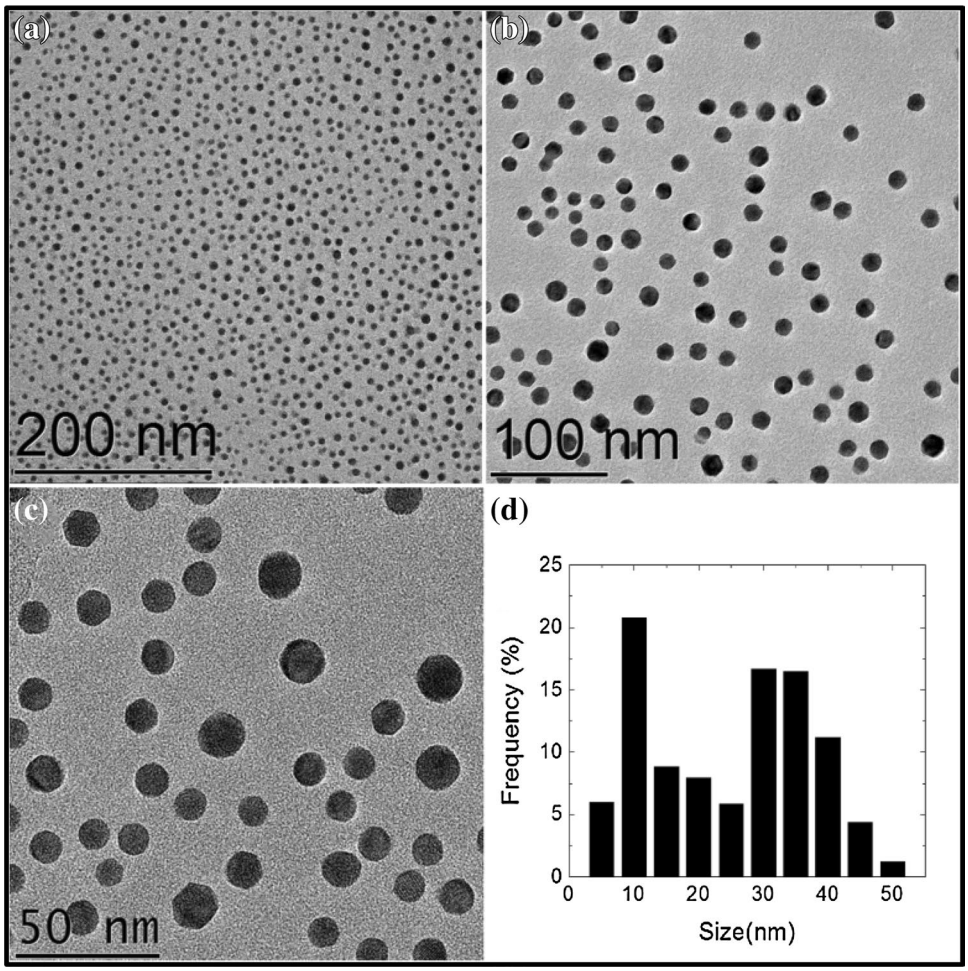

Fig. 6 **a–c** Low magnification TEM image, **d** size distribution of the sample

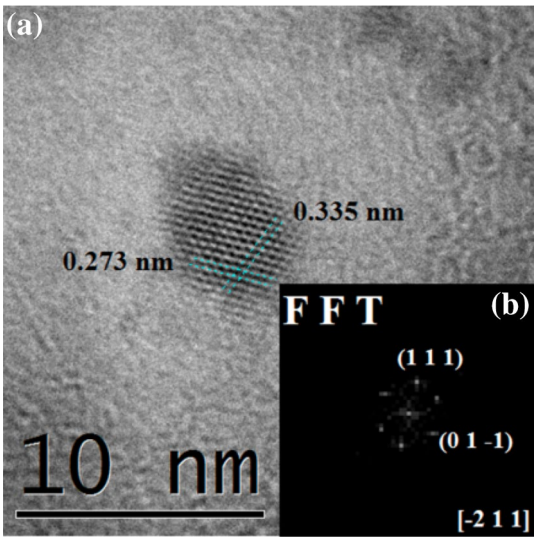

Fig. 7 **a** HREM images of individual nanoparticle and **b** their corresponding FFT

agreement with the crystallite size was also calculated from XRD data.

In Fig. 7 high resolution electron microscopy (HREM) is presented. The structure is clearly resolved; so a discrete Fourier transform Fig. 7b (using a Fast Fourier Transform algorithm, FFT) can be calculated and fed into our "DPIP" software to obtain crystallographic information [34]. Based on the analysis we conclude that the particles possess BiOCl tetragonal structure according to JCPDS: 96-901-1783. Figure 7a shows an individual nanoparticle of BiOCl in which the measured interplanar distances were $d_1 = 0.273$ nm, and $d_2 = 0.335$ nm, with an interplanar angle of $\theta_1 = 115.77°$, corresponding to the crystallographic planes (1 1 1), (0 1 −1), which theoretically have the following interplanar spacings: $d_{111} = 0.257$ nm and $d_{01-1} = 0.344$ nm, finally the nanoparticle is oriented in the zone axis [−2 1 1].

4 Conclusions

We have presented a simple and economic procedure to synthesize bismuth oxychloride (BiOCl) nanoparticles using tannic acid as stabilizing agent under highly acidic conditions. The particles were characterized by means of X-ray diffraction where the known main peaks could be identified. A characterization by means of Raman spectroscopy was done using three laser wavelengths, in which the characteristic reported vibrational modes of BiOCl were indexed. The high resolution transmission electron microscopy indicated that tetragonal BiOCl particles were formed.

Acknowledgements Our gratitude to Roberto Hernández Reyes for his aid with the Electron Microscope, Antonio Morales for X-Ray measurement at IFUNAM, and Cristina Zorrilla for her aid in the Advanced Materials laboratory. Also our gratitude to ICNAM of University of Texas at San Antonio, USA for the SEM images of the samples and finally the financial support from DGAPA with grant PAPIIT IN108915 is kindly acknowledged.

References

1. J. Yuan, J. Wang, Y. She, J. Hu, P. Tao, F. Lv, Z. Lu, Y. Gu, J. Power Sourc. **263**, 37–45 (2014)
2. X. Zhao, Z. Zhao, D. Wang, M. Fichtner, Angew. Chem. Int. Ed **52**, 13621–13624 (2013)
3. J. Li, Y. Yuab, L. Zhang, Nanoscale **6**, 8473 (2014)
4. F. Chen, H. Liu, S. Bagwasi, X. Shen, J. Zhang, J. Photochem. Photobiol. A, **215**, 76–80 (2010)
5. L. Zhang, W. Wang, D. Jiang, E. Gao, S. Sun, Nano Res. **8**, 821–831 (2015)
6. K. Zhang, C. Liu, F. Huang, C. Zheng, W. Wang, Appl. Catal., B **68**, 125–129 (2006)
7. L. Armelao, G. Bottaro, C. Maccatoc, E. Tondello, Dalton Trans **41**, 5480 (2012)
8. S. Kang, R. C. Pawar, Y. Pyo, V. Khare, C. Sunyong, J. Exp. Nanosci. **11**, 259–275 (2015)
9. J. Yu, B. Wei, L. Zhu, H. Gao, W. Sun, L. Xu, Appl. Surf. Sci **284**, 497–502 (2013)
10. I.D. Sharma, G. Kant, V. Kumar, S.N. Tripathi, R. Kurchania, C. Kant, A. Kumar, S.K.K. Cogent, Chemistry **1**, 1076371 (2015)
11. P. Jagdalea, M. Castellinob, F. Marrecc, S.E. Rodil, A. Tagliaferro, Appl. Surf. Sci **303**, 250–254 (2014)
12. M. Gao, D. Zhang, X. Pu, M. Li, Y. Moon, J. Jeong, P. Cai, S. Kim, H. Jin, J. Am. Ceram. Soc **98**, 1515–1519 (2015)
13. S. Wu, C. Wang, Y. Cui, W. Hao, T. Wang, P. Brault, Mater. Lett. **65**, 1344–1347 (2011)
14. S. Xi Zhoua, Y. Ke, J. Lia, S. Lu, Mater. Lett. **57**, 2053–2055 (2003)
15. K. Ren, J. Liu, J. Liang, K. Zhang, X. Zheng, H. Luo, Y. Huang, P. Liu, X. Yu, Dalton Trans. **42**, 9706–9712 (2013)
16. B. Sarwan, B. Pare, A.D. Acharya, Mater. Sci. Semicond. Process. **25**, 89–97 (2014).
17. X. Du, W. Zhao, Y. Liu, X. Huang, F. Mao, Adv. Mater. Res. **487**, 841–844 (2012)
18. A. Tadjarodi, O. Akhavan, K. Bijanzad, M.M. Khiavi, Monatsh Chem. **147**, 685–696 (2016)
19. H. Jia-jia, L. Jia-qin, R. Li-li, B. Hai-dong, Z. Xin-yi, W. Yu-cheng. Optoelectron. Lett. **11**, 6–9 (2015)
20. X. Xiao, R. Hao, M. Liang, X. Zuo, J. Nan, L. Li, W. Zhang, J. Hazard. Mater **233–234**, 122–130 (2012)
21. Y. Li, J. Liu, J. J. Jiang, Yu. Dalton Trans. **40**, 6632 (2011)
22. Z. Cui, L. Mi, D. Zeng, J. Alloys Compd. **549**, 70–76 (2013)
23. J. Cheng, C. Wang, Y. Cui, Y. Sun, Y. Zuo, J. Mater. Sci. Technol. **30**, 1130–1133 (2014)
24. S. Cao, C. Guo, Y. Lv, Y. Guo, Q. Liu, Nanotechnology **20**, 275702 (2009)
25. X. Hu, Y. Xu, H. Zhu, F. Hua, S. Zhu. Mat. Sci. Semicon. Proc. **41**, 12–16 (2016)
26. X. Zhang, X. Wang, L. Wang, W. Kang, L. Long, W. Li, H. Yu. Appl. Mater. Interfaces **6**, 7766–7772 (2014)
27. R. Herrera-Becerra, J.L. Rius, C. Zorrilla, Appl Phys A **100**, 453–459 (2010)
28. W. Abdelwahed, G. Degobert, S. Stainmesse, H. Fessi, Adv. Drug. Deliv. Rev. **58**, 1688–1713 (2006).

29. A.F.M. Ascencio, R.H. Becerra, Appl. Phys. A. **119**, 909–915 (2015)
30. J. Bergmann, P. Friedel, R. Kleeberg. IUCr Commission on Powder Diffraction Newsletter, No. 20, pp. 5–8 (1998)
31. N. Döbelin, R. Kleeberg, J. Appl. Crystallogr. **48**, 1573–1580 (2015)
32. M.P. Klug, L.E. Alexander. Wiley, 2nd Edition, p. 634 (1974)
33. A. Rulmont, Spectrochim. Acta, Part A. 30 311–313 (1974)
34. R. Galicia, R. Herrera, J. Rius, C. Zorrilla, A. Gómez, Rev. Mex. Fís. 59, 102–106 (2013)